ICMIEE-PI-140283

Numerical investigation of natural convection heat transfer of nanofluids inside a wavy cavity

*Md. Maruf Billah[1] , Neethila Nabanita Poddar[1] and Md. Mamun Molla[3]**
[1,2]Dept. of Electrical and Computer Engineering, North South University, Dhaka-1229, BANGLADESH
[3*]Dept. Mathematics and Physics, North South University, Dhaka-1229, BANGLADESH

ABSTRACT
In this research, heat transfer efficiency of nanofluids, through natural convection, inside a sealed wavy cavity has been examined numerically. Copper has been used as nanoparticles for primary investigation, with water as the base fluid. The governing Navier-Stokes and energy equations have been transformed into Cartesian curvilinear coordinates and then solved numerically using the finite volume method imposing several boundary conditions. Numerical code written in FORTRAN programming language is used to simulate the dimensionless, discretized governing equations. The study has been conducted for a range of Rayleigh numbers ($10^3 < Ra < 10^6$) and different volume fractions ($0 < \phi < 0.2$). The code is validated with previous published results and found to be in good agreement. The obtained results are illustrated in terms of the isotherms, streamlines, velocity and temperature profiles as well as the rate of heat transfer. It is observed that volume fraction of nanoparticles and the Rayleigh number affect the flow and heat transfer characteristics of nanofluids within the cavity.

Keywords: Nanofluids, Natural convection, curvilinear coordinates, Finite volume method, Wavy cavity.

1. Introduction
Heat transfer characteristics have been a major concern in the scientific world and have been the focus of many scientific researches because many devices and equipments starting from major industrial machines to the computers at home require cooling. For most of those equipments, like a flat-plate solar collector or a solar thermal collector, the performance improves with the increase in heat transfer efficiency. The conventional heat transfer materials like water, air, ethylene glycol, engine oil and so on were used as coolants but they have their limitations. The lower heat transfer performances of these conventional fluids obstruct the performance enhancement and compactness of heat exchangers. So the concept of nanofluid emerged which was first coined by Choi [1], a pioneer in this field.

Nanofluids are dispersion of nanometer sized particles (nanoparticles) in the conventional base fluids mentioned above. Nanoparticles can be metallic and non-metallic and may contain aluminum, copper, titanium etc. These suspensions of nanoparticles in base fluids have been reported to have increased the heat transfer characteristics of the fluids and thus enhance the efficiency of the system. This increase in heat transfer is mainly due to high thermal conductivity of the nanoparticles. Xuan and Li [2] conducted theoretical study to find that the heat transfer increases with the introduction of nanoparticles. Minsta et al. [3] and Pang et al. [4] also showed the enhancement of thermal conductivity of nanofluids in their research. Many studies and research works have been done on nanofluids to understand their characteristics properly. There were numerical and experimental works on nanofluids with various geometries such as, square cavity (Esmaeil [5]), triangular cavity (Yu et al. [6]), pipe (Abouali et al. [7]), inclined angle (Oztop [8]) and so on, and with various governing parameters (Rayleigh number, volume fraction, Grashof number, etc).

The literature reviewed reveals that many efforts were given to understand the characteristic of the nanofluids. Many studies were done with square cavity. Khanafer et al. [9] was one of the first to use nanofluids inside the cavity and his work was extended by Violi et al. [10] for square cavity. As the literature review suggests, there were also some works on square cavity with wavy wall, like Abu Nada et al. [11], Farhadi et al. [12], Mansour et al. [13] and Sonam singh et al. [14]. These papers studied the different parameters of nanofluids in different geometries of wavy wall cavity to understand their effects. However, to the best knowledge so far, none of them did any study on natural convection flow with left wall heated wavy and right wall cold wavy and top and bottom adiabatic flat.
So the main aim of this study is to investigate the effects of vertical wavy walls, heated from the left, on the flow of the nanofluids and the effects on the heat transfer characteristics of the nanofluids. This study intends to draw a qualitative comparison, based on the simulation findings, between flat and wavy walls. A mathematical model has been developed, based on which the simulations are done and the results are discussed.

2. Mathematical modeling
A two-dimensional (2D) rectangular cavity of height H and width L *is* considered for the present study. The top and bottom wall is entirely adiabatic. No-slip and no penetration assumptions were imposed on the walls. The entire left sidewall is hot and the right sidewall is cool (see Fig. 1.). Considering this cavity contains nanofluid, which is Newtonian, incompressible laminar, to

*Corresponding author. Tel.: +88-02-8852000(Ext.1519); fax: +88-02-8823030
E-mail addresses: mmamun@northsouth.edu, mmamun@gmail.com

investigate the flow and thermal behavior when left wavy wall is heated under several conditions.

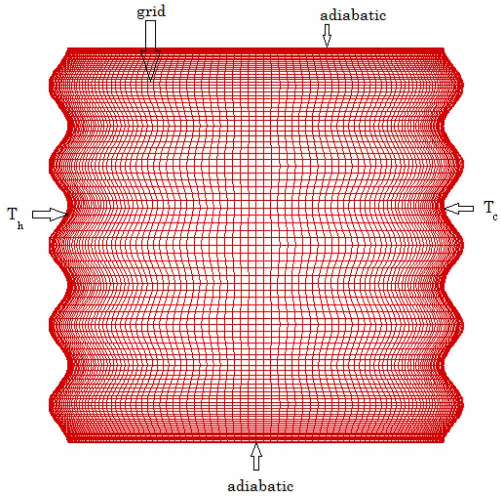

Fig. 1: Schematic for the physical model

The governing Navier-Stokes and energy equations for the present study taking into the account the Boussinesq approximation can be written as:

$$\frac{\partial u}{\partial x}+\frac{\partial v}{\partial y}=0 \tag{1}$$

$$\frac{\partial u}{\partial t}+u\frac{\partial u}{\partial x}+v\frac{\partial u}{\partial y}=-\frac{1}{\rho}\frac{\partial P}{\partial x}+\frac{\mu}{\rho}\left[\frac{\partial^2 u}{\partial x^2}+\frac{\partial^2 u}{\partial y^2}\right] \tag{2}$$

$$\frac{\partial v}{\partial t}+v\frac{\partial v}{\partial y}+u\frac{\partial v}{\partial x}=-\frac{1}{\rho}\frac{\partial P}{\partial y}+\frac{\mu}{\rho}\left[\frac{\partial^2 v}{\partial y^2}+\frac{\partial^2 v}{\partial x^2}\right]+g\beta(T-T_\infty) \tag{3}$$

$$\frac{\partial T}{\partial t}+u\frac{\partial T}{\partial x}+v\frac{\partial T}{\partial y}=\kappa\left[\frac{\partial^2 T}{\partial x^2}+\frac{\partial^2 T}{\partial y^2}\right] \tag{4}$$

The boundary conditions for the present investigation are presented as:

Left wall: at $x = 0$, $0 \le y \le 1$: $T = 1$, $u = v = 0$

Right wall: at $x = 1$, $0 \le y \le 1$: $T = 0$, $u = v = 0$

Top wall: at $y = 1$, $0 \le x \le 1$: $\frac{\partial T}{\partial y}=0$, $u = v = 0$

Bottom wall: at $y = 0$, $0 \le x \le 1$: $\frac{\partial T}{\partial y}=0$, $u = v = 0$

It is important that the terms in our equation are in a form that is independent of the dimensions of the geometry and hence is feasible for comparison. So the governing equations are non-dimensionalized using the following dimensionless parameters.

$$\left.\begin{aligned} &X=\frac{x}{L},\ Y=\frac{y}{L},\ U=\frac{uL}{\alpha_f},\ V=\frac{vL}{\alpha_f},\ \Theta=\frac{T-T_c}{T_h-T_c},\ P=\frac{pL^2}{\rho_f\alpha_f^2} \\ &Pr_f=\frac{\nu_f}{\alpha_f},\ Ra=\frac{g\beta(T_h-T_c)L^3 Pr_f}{\nu_f^2},\ \tau=\frac{\alpha_f t}{L^2},\ \nu_{nf}=\frac{\mu_{nf}}{\rho_{nf}},\ \alpha_{nf}=\frac{K_{nf}}{(\rho c_p)_{nf}} \end{aligned}\right\} \tag{5}$$

Here, the effective viscosity for a suspension containing small spherical solid nanoparticles is given as μ_{nf} and the effective density of a fluid containing solid nanoparticles is given by ρ_{nf} .

The dimensionless governing equations is of the following form,

$$\frac{\partial U}{\partial X}+\frac{\partial V}{\partial Y}=0 \tag{6}$$

$$\frac{\partial U}{\partial \tau}+U\frac{\partial U}{\partial X}+V\frac{\partial U}{\partial Y}=-\frac{1}{(1-\phi)+\phi\frac{\rho_s}{\rho_f}}\frac{\partial P}{\partial X}+ \Pr\frac{1}{(1-\phi)^{2.5}\left[(1-\phi)+\phi\frac{\rho_s}{\rho_f}\right]}\left[\frac{\partial^2 U}{\partial X^2}+\frac{\partial^2 U}{\partial Y^2}\right] \tag{7}$$

$$\begin{aligned}\frac{\partial V}{\partial \tau}+U\frac{\partial V}{\partial X}+V\frac{\partial V}{\partial Y}=&-\frac{1}{(1-\phi)+\phi\frac{\rho_s}{\rho_f}}\frac{\partial P}{\partial Y}+\frac{\Pr}{(1-\phi)^{2.5}\left[(1-\phi)+\phi\frac{\rho_s}{\rho_f}\right]}\left[\frac{\partial^2 V}{\partial X^2}+\frac{\partial^2 V}{\partial Y^2}\right]+\\ &Ra\Pr\Theta\left[\frac{1}{1+\frac{(1-\phi)\rho_f}{\varphi\rho_s}}\frac{\beta_s}{\beta_f}+\frac{1}{1+\frac{\phi\rho_s}{(1-\phi)\rho_f}}\right]\end{aligned} \tag{8}$$

$$\frac{\partial \Theta}{\partial \tau}+U\frac{\partial \Theta}{\partial X}+V\frac{\partial \Theta}{\partial Y}=\frac{\frac{K_{nf}}{K_f}}{\left[(1-\phi)+\phi\frac{(\rho C_p)_s}{(\rho C_p)_f}\right]}\left[\frac{\partial^2 \Theta}{\partial X^2}+\frac{\partial^2 \Theta}{\partial Y^2}\right] \tag{9}$$

3. Numerical method and validation

The governing equations (6)-(9) were transformed to curvilinear coordinates $x=x_1=(\zeta_1,\zeta_2)$ and $y=x_2=(\zeta_1,\zeta_2)$ so that complex geometry can be handled. The determinant of the Jacobian matrix, J, is defined as :

$$|J|=\begin{vmatrix}\frac{\partial x_1}{\partial \zeta_1} & \frac{\partial x_1}{\partial \zeta_2}\\ \frac{\partial x_2}{\partial \zeta_1} & \frac{\partial x_2}{\partial \zeta_2}\end{vmatrix} \quad \text{Therefore,} \quad |J|=\frac{\partial x_1}{\partial \zeta_1}\frac{\partial x_2}{\partial \zeta_2}-\frac{\partial x_1}{\partial \zeta_2}\frac{\partial x_2}{\partial \zeta_1} \tag{10}$$

$$|J|=\frac{\partial x_i}{\partial \zeta_j}A_{ij}\text{, where } A=\begin{vmatrix}\frac{\partial x_2}{\partial \zeta_2} & -\frac{\partial x_2}{\partial \zeta_1}\\ -\frac{\partial x_1}{\partial \zeta_1} & \frac{\partial x_1}{\partial \zeta_2}\end{vmatrix}$$

The final transformed equation into curvilinear coordinate are:
Continuity Equation:

$$\frac{A_{11}}{|J|}\frac{\partial U}{\partial \zeta_1}+\frac{A_{12}}{|J|}\frac{\partial U}{\partial \zeta_2}+\frac{A_{21}}{|J|}\frac{\partial V}{\partial \zeta_1}+\frac{A_{22}}{|J|}\frac{\partial V}{\partial \zeta_2}=0 \qquad (11)$$

Momentum equation:
U-momentum

$$\frac{\partial U}{\partial \tau}+\frac{1}{|J|}(UA_{11}+VA_{21})\frac{\partial U}{\partial \zeta_1}+\frac{1}{|J|}(UA_{12}+VA_{22})\frac{\partial U}{\partial \zeta_2}=-\frac{1}{\left[(1-\phi)+\frac{\phi\rho_s}{\rho_f}\right]}\left[\frac{A_{11}}{|J|}\left(\frac{\partial P}{\partial \zeta_1}\right)+\frac{A_{12}}{|J|}\left(\frac{\partial P}{\partial \zeta_2}\right)\right]+\Pr\frac{1}{(1-\phi)^{2.5}\left[(1-\phi)+\phi\frac{\rho_s}{\rho_f}\right]\left|J^2\right|}\left[\begin{aligned}&\left(A_{11}^2+A_{21}^2\right)\frac{\partial^2 U}{\partial \zeta_1^2}+2(A_{11}A_{12}+A_{21}A_{22})\frac{\partial^2 U}{\partial \zeta_1\partial \zeta_2}\\&+\left(A_{12}^2+A_{22}^2\right)\frac{\partial^2 U}{\partial \zeta_2^2}\end{aligned}\right] \qquad (12)$$

$$\frac{\partial V}{\partial \tau}+\frac{1}{|J|}(UA_{11}+VA_{21})\frac{\partial V}{\partial \zeta_1}+\frac{1}{|J|}(UA_{12}+VA_{22})\frac{\partial V}{\partial \zeta_2}=-\frac{1}{\left[(1-\phi)+\frac{\phi\rho_s}{\rho_f}\right]}\left[\frac{A_{11}}{|J|}\left(\frac{\partial P}{\partial \zeta_1}\right)+\frac{A_{12}}{|J|}\left(\frac{\partial P}{\partial \zeta_2}\right)\right]+\Pr\frac{1}{(1-\phi)^{2.5}\left[(1-\phi)+\phi\frac{\rho_s}{\rho_f}\right]\left|J^2\right|}\left[\left(A_{11}^2+A_{21}^2\right)\frac{\partial^2 V}{\partial \zeta_1^2}+2(A_{11}A_{12}+A_{21}A_{22})\frac{\partial^2 V}{\partial \zeta_1\partial \zeta_2}+\left(A_{12}^2+A_{22}^2\right)\frac{\partial^2 V}{\partial \zeta_2^2}\right]+Ra\Pr\Theta\left[\frac{1}{1+\frac{(1-\phi)\rho_f}{\phi\rho_s}}\frac{\beta_s}{\beta_f}+\frac{1}{1+\frac{\phi\rho_s}{(1-\phi)\rho_f}}\right] \qquad (13)$$

Internal energy equation:

$$\frac{\partial \Theta}{\partial \tau}+\frac{1}{|J|}\frac{\partial \Theta}{\partial \zeta_1}(UA_{11}+VA_{21})+\frac{1}{|J|}\frac{\partial \Theta}{\partial \zeta_1}(UA_{12}+VA_{22})=\frac{\frac{K_{nf}}{K_f}}{\left[(1-\phi)+\phi\frac{(\rho C_p)_s}{(\rho C_p)_f}\right]|J|^2}\left\{\begin{aligned}&\left[\frac{\partial^2\Theta}{\partial \zeta_1^2}\right]\left(A_{11}^2+A_{21}^2\right)+\left[\frac{\partial^2\Theta}{\partial \zeta_2^2}\right]\left(A_{12}^2+A_{22}^2\right)\\&+2\frac{\partial^2\Theta}{\partial \zeta_1\partial \zeta_2}(A_{11}A_{12}+A_{21}A_{22})\end{aligned}\right\} \qquad (1ss4)$$

The transformed equations (11-14) were discretized using finite volume method. The discretized governing equations were used for simulation in code written in FORTRAN programming language.

The present code was tested for grid independence using three different grid arrangements: 81×81, 101×101 and 121×121. Temperature profiles are plotted at mid section of cavity for Ra=10^5, ϕ =10% and Pr =6.2, as illustrated by Figure 2. It is observed that the shape of the curve changes consistently for all three grid sizes, which shows that grid independence, has been established.

Moreover the numerical codes were validated with the benchmark results of de Vahl Davis [15], as shown by table 1 and were found to be in good agreement.

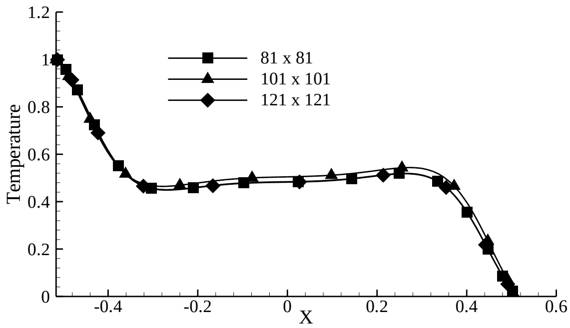

Fig.2 Temperature profiles at mid section of cavity for different grid combinations

Table1 Validation of present study with benchmark results of Davis [15] in terms of the average Nusselt number Nu_{avg} for the pure fluid

Ra	10^4	10^5	10^6
Present	2.45	4.49	8.78
Davis [15]	2.24	4.52	8.80

4. Results and Discussion

In this section**,** numerical results for the streamlines and isotherms contours as well as temperature, velocity and local Nusselt number profiles have been presented graphically that demonstrate the effects of the controlling parameters namely solid volume fraction ($0 \le \phi \le 0.2$) and the Rayleigh number ($10^4 \le Ra \le 10^6$).

4.1 Isotherms and streamlines

Fig. 3 illustrates comparison of the isotherms (on the left) and streamlines (on the right) between nanofluid (ϕ = 0.2) and pure fluid (ϕ = 0) for Rayleigh numbers 10^4 to 10^6. As seen in the diagrams (Fig. 3), for low Rayleigh numbers (*Ra* =10^4), the isotherms are distributed approximately parallel to the vertical wavy walls. As Rayleigh number increases, the isotherms become horizontal at the central region of the cavity and vertical at the thin boundary layers. This behavior occurs because at a low *Ra* value, the heat transfer is only due to conduction between the hot and the cold walls. However, with increase in *Ra*, the heat transfer is done by convection rather than conduction due to increased buoyancy. It is also observed that the left and right wavy walls affect the shape of the isotherms and streamlines.

As illustrated in the Fig. 3, at Ra=10^4, an oval shaped cell is formed in the clockwise direction with $\psi_{\min}$ = -0.0154747 for pure fluid and $\psi_{\min}$ = -0.00860596 for nanofluid (ϕ = 0.2). As Rayleigh number increases, the length of central vortex increases and the streamlines elongate parallel to the horizontal walls for both pure and nanofluids. At *Ra* =10^6, $\psi_{\min}$ = -1.88113 for pure fluid and $\psi_{\min}$ = -1.05468 for nanofluid. This shows that absolute value of stream function increases with Rayleigh number but decreases with particle volume fraction. Moreover, it is observed that at $Ra = 10^6$, the central vortex of the pure fluid occupies a larger area than that of nanofluid. The central streamline contour of nanofluid becomes divided into two distinct vortices, whereas the central vortex for pure fluid does not break up. Similar results were obtained by Khanafer et al. [9] for the flat square cavity, which attributed this behavior to the dispersion effect. It is clearly observed that as Rayleigh number increases, boundary layers become thinner and denser causing steeper velocity and temperature gradients near the boundary. With higher Rayleigh number, the streamline gradient increases, representing an increase in velocity and an enhancement of the absolute circulation strength of the fluid flow.

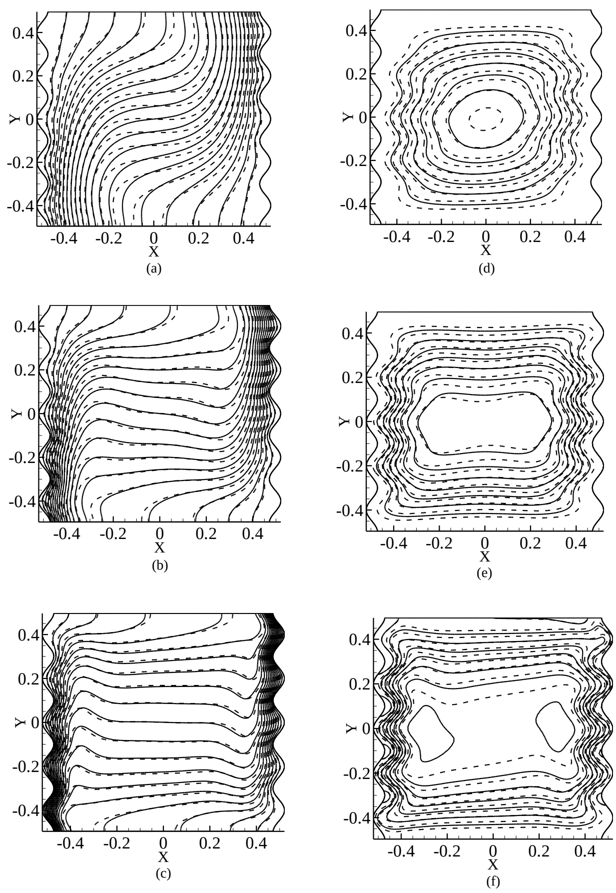

Fig.3 Comparison between nanofluid (-) (ϕ = 0.2) and pure fluid (- - -) (ϕ = 0) for isotherms at Rayleigh Numbers (a) 10^4 (b) 10^5 (c) 10^6 and for streamlines at Rayleigh numbers (d) 10^4 (e) 10^5 (f) 10^6

4.2 Vertical and horizontal velocity profiles

To demonstrate the effects of Rayleigh number and volume fraction on fluid flow, velocity profiles are plotted at mid planes of the wavy enclosure. The Figs.4 (a)-(b) show that the velocity profiles undergo a parabolic variation near the adiabatic and isothermal walls respectively. In addition, the velocities at the center of the enclosure and at the walls are almost zero compared to those at the boundaries near the walls, where fluid flow occurs at higher velocities.

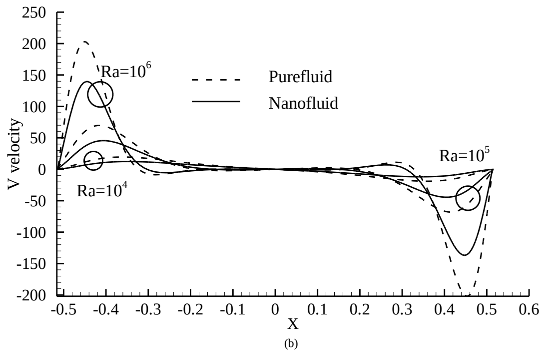

Fig.4 Comparison of vertical velocity profiles for nanofluid (-) and pure fluid (- - -) at mid section of cavity for different Rayleigh numbers.

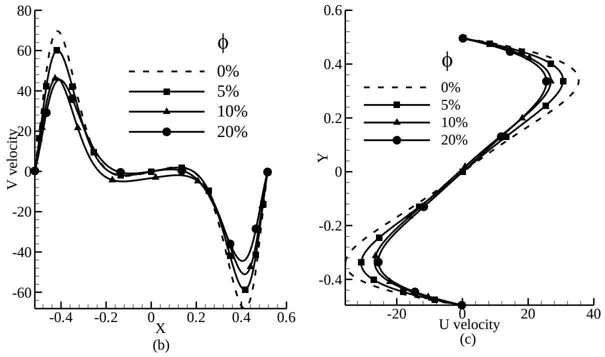

Fig.5 Comparison of vertical and horizontal velocity profiles for nanofluid (-) and pure fluid (- - -) at mid section of cavity for different volume fraction and at Ra= 10^5.

This is due to the fact that no-slip and no penetration assumptions are imposed on the walls. From Fig. 5, it is observed that for ϕ= 0, the maximum stream function value is obtained as $\psi_{\max}$ = 5.09334 at $Ra = 10^4$. When solid volume fraction is increased to ϕ = 0.05, the maximum value of stream function decreases to $\psi_{\max}$ = 4.48676. Similar trend is also found for $Ra = 10^5$ and $Ra = 10^6$. This shows that the absolute magnitudes of both vertical and horizontal velocities decrease with increasing volume fraction. This is because increase in volume fraction causes decrease in intensity of buoyancy and thereby reduces fluid flow intensity. Similar results were found in many previous studies (Mansour et al. [13]) with various geometries and conditions.

4.3 Nusselt number

From Table 2, it is evident that the average Nusselt number Nu_{avg} increases with increase in Rayleigh number and volume fraction. This observation is in agreement with other research works (Khanafer et al. [9], Abu-Nada et al. [10], and Violi et al. [11]). As volume fraction of nanoparticles increases, the divergence in average Nusselt number becomes greater especially for higher Rayleigh numbers due to predominant effects of convective heat transfer. Use of nanoparticles in fluid increases the Nu number by about 34% for Ra =10^5 and 35% for Ra =10^6 at ϕ = 0.2 compared to pure fluid. The results indicate that with increase in particle concentration, thermal conductivity in fluid improves, thereby causing an enhancement in mean *Nu* number (heat transfer performance).

Table 2 Variation of Average Nusselt number for different values of volume fraction and Rayleigh numbers.

Nu_{avg}	$Ra= 10^4$	$Ra=10^5$	$Ra= 10^6$
ϕ = 0%	1.7731	3.7182	7.3324
ϕ = 5%	2.0498	4.2925	8.4736
ϕ = 10%	2.2885	5.3791	9.5124
ϕ = 20%	2.6769	5.6643	11.327

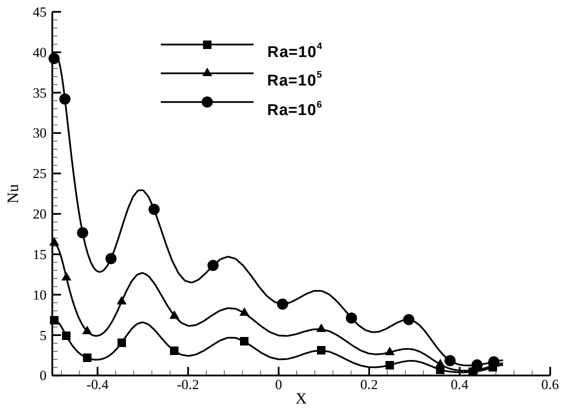

Fig.6 Variation of local Nusselt number with Rayleigh number at ϕ = 0.2.

From Fig. 6, it is observed that the lowest heat transfer occurs at Ra =10^4 and the highest heat transfer is observed at Ra =10^6. By definition, *Nu* number is the ratio of convective to conductive heat transfer. As described earlier, for low Rayleigh numbers, heat transfer within the cavity is dominated by conduction because viscous force is greater than buoyancy force.

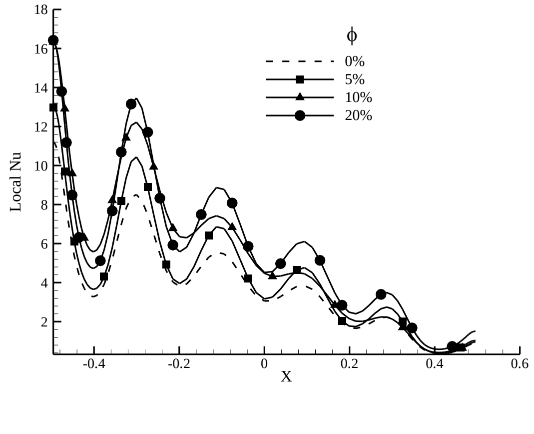

Fig. 7 Variation of local Nusselt number with volume fraction at Ra=10^5.

Hence the value of *Nu* is lower and variation is less for Ra =10^4. As *Ra* increases, a stronger buoyancy effect is induced and greater thermal energy transfer occurs, causing an increase in Nu. Moreover, Fig. 7 illustrates that the use of nanoparticles gives rise to higher *Nu* compared to pure fluid for the same *Ra*, indicating improvement of heat transfer with increase in volume fraction.

4.4 Comparison between different nanoparticles

Fig. 8 demonstrates variation of local Nusselt number for three different nanoparticles- Cu, Al_2O_3 and TiO_3. It is clearly observed that the highest heat transfer occurs for Cu and the lowest for TiO_3. This is because TiO_3 has the lowest thermal conductivity (Ks) compared to Cu and Al_2O_3. Hence the results reinforce that in comparison to the other two nanoparticles, Cu is more feasible due to higher enhancements of heat transfer.

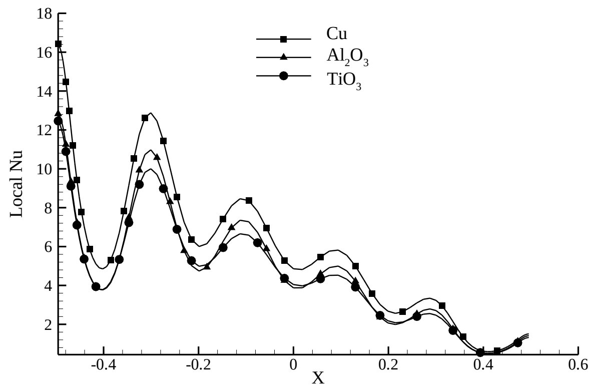

Fig.8 Variation of local Nusselt number for different nanoparticles at Ra = 10^5 and ϕ = 0.2.

4.5 Comparison between flat and wavy surface heating

Fig. 9 shows that the shape of local *Nu* profile is strongly dependant on the geometry of the enclosure.

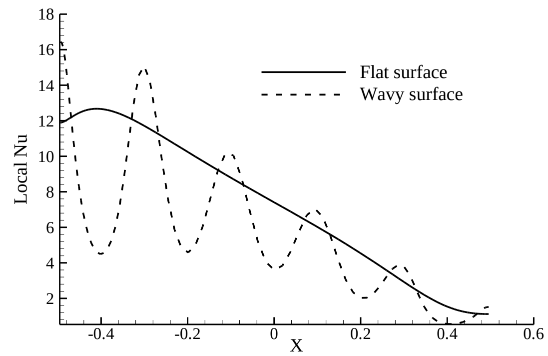

Fig. 9 Variation of local Nusselt number for wavy and flat surface heating

Table 3 Percentage difference of average Nu_{avg} for flat and wavy surface heating

	Wavy	Flat	% difference
Nu_{avg}	5.6643	7.2743	22.132

In case of the wavy surface, the local Nusselt number value changes continuously depending on the shape of the heated surface. Table 3 reveals one important finding that the average Nusselt number decreases and is almost 22% less for a wavy wall compared to a flat surface. This is because, a cavity with wavy walls have a larger surface area than that for flat walls. However, at the boundary, the local Nusselt number for wavy-wall shows almost 37% increase than the flat wall, indicating a much higher heat transfer with increased convection due to increased buoyancy force. The wavy wall of the geometry used is a sine function with amplitude of 0.05. Although the local Nusselt number for wavy wall decreases rapidly than that of flat wall, it has certain peak regions where heat transfer is more than the non-wavy surfaces. These are the regions where the local Nusselt numbers are higher for wavy surfaces.

4.6 Comparison between aspect ratio A =1 and A = 0.5

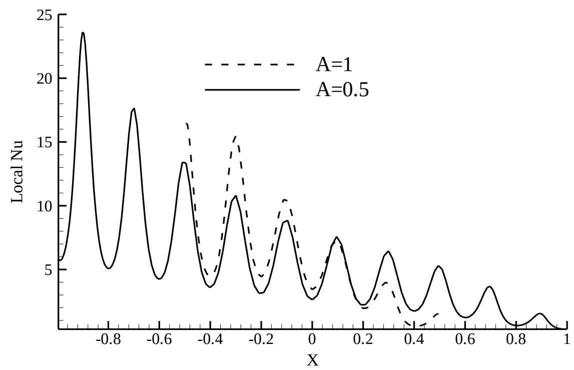

Fig. 10 Variation of local Nusselt number with aspect ratio at $Ra = 10^5$ and ϕ =0.2.

The variation of the local Nusselt number for the two different aspect ratios is compared in Fig.10. The solid lines represents aspect ratio A =0.5 and the dotted line represents aspect ratio A =1. The overall pattern of the two graphs is similar, and in both the graphs local Nusselt number variation is sinusoidal. This variation is due to the wavy surface pattern of the left heated wall. However, it is evident from the graph that the highest heat transfer, at a particular instance, takes place with the aspect ratio A = 0.5 near the boundary. The maximum value of local Nusselt number for A = 0.5 is 24. Whereas, the maximum value for A =1 is 17, which is about 29% lower than that for aspect ratio A = 0.5.

5. Conclusion

The results found show that the nanofluids exhibit much better heat transfer efficiency, in terms of average Nusselt number, than the purefluids in case of the wavy cavity. Similar heat transfer efficiency increment, for nanofluids, is also found in the literature for flat surface cavity. In this research work, it has been found that the streamline contours, temperature profiles, average Nusselt number and local Nusselt number are affected by the wavy surface of the cavity. In particular, the local Nusselt number varies much with the wavy surface. It is observed that the flow rate for both pure fluid and nanofluid increases with the increase in Rayleigh number, but the flow rate of pure fluid is higher than the nanofluid at all Rayleigh numbers. Also the absolute magnitude of both vertical and horizontal velocities decreases with the increase of volume fraction, from φ = 0 to ϕ = 0.2. The heat transfer efficiency, depicted by Nusselt number, seems to increase with the increase in Rayleigh number, Ra =10^4 to Ra =10^6, for each volume fraction. Moreover, the Nusselt number increases with the increase in volume fraction. It was found that, the use of nanoparticles of volume fraction ϕ = 0.2, increases the Nusselt number by 34% for Ra =10^5 and 35% for Ra =10^6, compared to that of pure fluids. This shows an increase in heat transfer efficiency for nanoparticles. However, if these results of wavy surface are compared with that of flat surface, then a decrease in average Nusselt number, by 22%, for the wavy surface is observed. Although the local Nusselt number shows certain places with higher heat transfer efficiency, as high as 37% than the flat surface, the overall heat transfer is assumed to have decreased for the wavy surface.

Moreover, while focusing on different nanoparticles and the aspect ratios, it was found that Copper has the highest Nusselt number which is 5.66 among the three nanoparticles used, which in turn shows that Copper has the highest heat transfer rate. Change in aspect ratio also changes the heat transfer rate. If a nanofluid, having a nanoparticle of volume fraction ϕ = 0.2, is considered, then the value of average Nusselt number for A = 0.5 will be 29% more than that of A =1. This shows a much higher heat transfer occurs for a lower aspect ratio.

NOMENCLATURE

A : cofactor
C_p : specific heat (J kg^{-1} K^{-1})
g : gravitational accleration (m s^{-2})
J : Jacobian
K_f : fluid thermal conductivity (W $m^{-1}K^{-1}$)
K_{nf} : nanofluid thermal conductivity (W $m^{-1}K^{-1}$)
L : reference lenght (m)
Nu : Nusselt number
Nu_{avg} : average Nusselt number
Pr : Prandlt number
P : dimensionless pressure
p : dimensional pressure (N m^{-2})
Ra : Rayleigh number
T : dimensional temperature (K)

u,v : dimensional velocity components (m .S^{-1})
U,V : dimensionless velocity components
x,y : Cartesian coordinates (m)
X,Y : dimensionless coordinates
Greek symboles
Θ : non dimensional temperature (K)
ϕ : solid volume fraction
ψ : streamline function, (Ψ/α_f)
β : thermal expansion coefficient, (k^{-1})
β_{nf} : nanofluid thermal expansion coefficient, (k^{-1})
τ : non dimensional time ($T-T_c/\Delta T$)
α : thermal diffusivity, ($m^2\ s^{-1}$)
ν : kinematic viscosity, ($m^2\ s^{-1}$)
μ : dynamic viscosity, (kg $m^{-1}\ s^{-1}$)
$\zeta_1\ \zeta_2$: dimensionless coordinates in Jacobian transformation

REFERENCE

[1] S. U. Choi, J. Eastman, Enhancing thermal conductivity of fluids with nanoparticles. *International Mechanical Engineering Congress and Exhibition*, San Francisco, USA, November 12-15 (1995).

[2] Y. Xuan, Heat Transfer Enhancement Of Nanofluids. *International Journal of Heat and Fluid Flow*, *21*(1), 58-64. (2000).

[3] H. Mintsa, G. Roy, C. Nguyen, D. Doucet, New temperature dependent thermal conductivity data for water-based nanofluids, *Int. J. Thermal Sciences*, 48 (2009) 363-371.

[4] C. Pang, J. Jung, J. W. Lee, Y. T. Kang, Thermal conductivity measurement of methanol-based nanofluids with Al_2O_3 and SiO_2 nanoparticles. *International Journal of Heat and Mass Transfer*, *55*, 5597-5602. (2012).

[5] K. Esmaeil, Numerical feasibility study of utilizing nanofluids in laminar natural convection inside enclosures. *Heat and Mass Transfer*, *49*, 41-54. (2012).

[6] Z. Yu, X. Xu, Y. Hu, L. Fan, K. Cen, Numerical study of transient buoyancy-driven convective heat transfer of water-based nanofluids in a bottom-heated isosceles triangular enclosure. *International Journal of Heat and Mass Transfer*, *54*(1-3), 526-532. (2011).

[7] O. Abouali, A. Falahatpisheh, Numerical investigation of natural convection of Al2O3 nanofluid in vertical annuli. *Heat Mass Transfer*, *43*, 15-24 (2009).

[8] Abu-Nada, E., & Oztop, H. F. (2009). Effects of Inclination Angle on Natural Convection in Enclosures Filled with Cu–water Nanofluid. *International Journal of Heat and Fluid Flow*, *30*(4), 669-678.

[9] K. Khanafer, K. Vafai, M. Lightstone, Buoyancy-driven heat transfer enhancement in a two-dimensional enclosure utilizing nanofluids, *International Journal of Heat and Mass Transfer* 46 (19) ,3639-3653. (2003).

[10] K. C. Lin, A. Violi, Natural convection heat transfer of nanofluids in a vertical cavity: Effects of non-uniform particle diameter and temperature on thermal conductivity, *International Journal of Heat and Fluid Flow* 31 (2), 236-245. (2010).

[11] E. Abu-Nada, H. F. Oztop, Numerical analysis of al2o3/water nanofluids natural convection in a wavy walled cavity, *Numerical Heat Transfer*, Part A: Applications 59 (5) 403-419 (2011).

[12] M. Jafari, M. Farhadi, K. Sedighi, E. Fattahi, Effect of wavy wall on convection heat transfer of water-al2o3 nanofluid in a lid-driven cavity using lattice boltzmann method, *International Journal of Engineering-Transactions* A: Basics 25 (2) (2012) 165.

[13] M. Mansour, M. Bakier, Free convection heat transfer in complex-wavy-wall enclosed cavity filled with nanofluid, *International Communications in Heat and Mass Transfer* 44 (2013) 108-115.

[14] S. Singh, R. Bhargava, Numerical study of natural convection within a wavy enclosure using mesh free approach: Effect of corner heating, *The Scientific World Journal* (2014).

[15] G. de Vahl Davis, Natural convection of air in a square cavity: a bench mark numerical solution, *International Journal for Numerical Methods in Fluids* 3 (3) 249-264. (1983).

[16] F.-H. Lai, Y.-T. Yang, Lattice boltzmann simulation of natural convection heat transfer of Al_2O_3 water nanofluids in a square enclosure, *International Journal of Thermal Sciences* 50 (10) 1930-1941. (2011)